Applied Catalysis B: Environmental 253 (2019) 263–270

Contents lists available at ScienceDirect

Applied Catalysis B: Environmental

journal homepage: www.elsevier.com/locate/apcatb

Self-limiting synthesis of Au–Pd core–shell nanocrystals with a near surface alloy and monolayer Pd shell structure and their superior catalytic activity on the conversion of hexavalent chromium

Xiaokun Li[a], Cuixia Li[b], Dong Xiang[a], Chunmei Zhang[a], Lu Xia[c], Xingyu Liu[c], Fuqin Zheng[a], Xiaoyu Xie[b], Youlin Zhang[b,*], Wei Chen[a,*]

[a] State Key Laboratory of Electroanalytical Chemistry, Changchun Institute of Applied Chemistry, Chinese Academy of Sciences, Changchun 130022, China
[b] State Key Laboratory of Luminescence and Applications, Changchun Institute of Optics, Fine Mechanics and Physics, Chinese Academy of Sciences, Changchun 130033, China
[c] China Electronics Technology Group Corporation No.49th Research Institute, Harbin 150001, China

ARTICLE INFO

Keywords:
Self-limiting
Core–shell nanocatalyst
Near surface alloy
Palladium monolayer
Hexavalent chromium conversion

ABSTRACT

In eliminating environmental chromium pollution, hexavalent chromium (Cr(VI)) reduction by HCOOH on Pd-based bimetallic/multimetallic nanocatalysts is attracting an increasing attention. However, it is still a challenge by precisely controlling the surface interface structure of the nanocrystals (NCs) to obtain highly efficient nanocatalysts on Cr(VI)) conversion. Here, a simple and robust synthesis method for Au-Pd core-shell NCs with a special interface structure has been developed by a novel self-limiting strategy. This interesting structure has a near surface alloy (NSA) of AuPd layer on Au core with outer surface of monolayer (ML) of Pd shell (denoted as NSA/ML), which is achieved only by one-pot synthesis. The self-limiting strategy is developed based on the unique catalysis reduction reaction of Au core, with which the growth of Pd shell is internally regulated by the surface Au atoms until the Au–Pd NCs with NSA/ML structure i.e. Au@AuPd@Pd_{ML} NCs are formed. Furthermore, the Au–Pd core–shell NCs with the shell from NSA to NSA/ML structure can be simply obtained by adjusting the added amount of Pd precursor. More importantly, the catalytic activities of Au–Pd NCs for the conversion of Cr(VI) to Cr(III) present a notable difference for the Pd in Au@AuPd and Au@AuPd@Pd_{ML} structures, and the Au@AuPd@Pd_{ML}NCs exhibited the superior catalytic activity for the conversion of Cr(VI). The present study demonstrates the core@NSA@$shell_{ML}$ is an efficient nanostructure to promote the catalytic performance of core–shell NCs for practical applications.

1. Introduction

It is well-known that hexavalent chromium (Cr(VI)) is one of the most common pollutants, which has been recognized as a strong carcinogen in the world, and very harmful to human health. Up to now, the conversion of Cr(VI) to Cr(III) has been considered as one of the most effective methods to eliminate the Cr pollution [1,2]. Among them, the reduction of Cr(VI) by formic acid (HCOOH) on Pd-based catalysts has attracted much attention owing to the simplicity, no secondary pollution and high efficiency [3–8]. However, its slow kinetics largely limit its practical applications in environmental remediation of Cr (VI) pollution. To this end, it is highly anticipated to exploit efficient strategies for designing more effective catalysts.

One of the successful strategies is to construct core-ultrathin shell (such as core@shell with a monolayer i.e. core@$shell_{ML}$) structured nanocomposites, because such structure holds the highest possible utilizing efficiency of shell materials [9–13]. More importantly, such nanostructures provide better opportunity to regulate their catalytic properties based on the ligand and strain effects [9,12–14]. However, the long-term performance stability needs to be considered because severe changes in surface composition arise due to metal migration during the catalytic reaction [14,15]. Lots of efforts have been devoted to reducing the structural deficiency of these nanocomposites. For the core@$shell_{ML}$ structured NCs, based on the difference in the surface energy and lattice constants, one of the effective ways to improve their catalytic performance is that an ultrathin near surface alloy (NSA) layer can be incorporated between the internal core and outer shell layer to form the core@NSA@$shell_{ML}$ nanostructures. For example, Xing et al.

* Corresponding authors.
E-mail addresses: zhangyl@ciomp.ac.cn (Y. Zhang), weichen@ciac.ac.cn (W. Chen).

https://doi.org/10.1016/j.apcatb.2019.04.071
Received 9 January 2019; Received in revised form 12 March 2019; Accepted 20 April 2019
Available online 25 April 2019
0926-3373/

have demonstrated that a PdAu alloy sublayer was incorporated between Au core and Pt monolayer to increase not only the durability, but also the catalytic activity of electrocatalysts [16]. In another article, it was also observed that alloyed AuPd@Pt_{ML} nanostructure showed minimal degradation over 100,000 cycles in fuel-cell stability tests [17]. Therefore, how to effectively control both the surface and interface structures in shell layer is important for designing highly efficient and stable core@shell catalysts.

Up to now, synthetic methods for the preparation of core@NSA@$shell_{ML}$ NCs are mainly based on two primary strategies. The first one is based on the underpotential deposition (UPD) approach, where a sacrificial metal is decorated onto the core surface by UPD, followed by galvanic displacement with shell precursors [16,17]. However, such approach is limited to the NCs on electrode surface and it is difficult to be applied on a large scale [9,12]. The second synthesis strategy employs a seed-mediated growth method, with which it is difficult to control the shell thickness due to the heterogeneity of core size and the inaccuracies of core concentration [9,18]. In addition, the synthesis process is often very complicated because external influence factors need to be accurately controlled, such as reaction temperature, precursor concentration, and reaction time [19–21]. For instance, to eliminate self-nucleation of the shell materials, the concentration of the precursor must be kept very low in reaction solution. In this context, the synthesis of core@NSA@$shell_{ML}$ NCs needs multistep fine control. Considering the above issues, a self-limiting method may be more attractive than the above synthesis approaches, because self-limiting route offers a more efficient, simple and self-controllable strategy for preparing core@shell nanomaterials with desired surface structure [22–24].

On the other hand, in the study of Au–Pd core–ultrathin shell structure, it was demonstrated by Wang et al. that with the Pd shell thicker than 2 nm, a AuPd alloy phase appeared in the interface between Au and Pd to release the interface strain induced by the lattice mismatch (4.6%) to form a Au@AuPd@Pd structure [25]. Whereas, the previous studies indicated that epitaxial growth of monolayer Pd shell on Au NCs will not induce a AuPd interlayer between Au core and Pd ML shell [9,12,25]. Based on the above discussion, we think that developing an appropriate method, for example, self-limiting strategy, to achieve Au–Pd NCs with Au@NSA@Pd_{ML} structure is very desirable. To this end, the major challenge is how to design the corresponding self-limiting route to obtain the anticipated nanostructure.

Inspired by our recent synthesis of Au@Pt core–shell NCs with Pt skin surface [26], here we designed a self-limiting strategy to synthesize Au@AuPd@Pd_{ML} NCs, based on the Au catalytic reduction reaction. In our self-limiting system, the Au NCs served as both the core seeds and catalyst, and a selected piperazine derivative (4-(2-hydroxyethyl)piperazine-1-(2-hydroxypropanesulfonic acid), HEPPSO) was used as the reductant for Pd precursor. Under Au core catalysis, the added Pd(II) ions were reduced to Pd atoms. It should be pointed out that the Pd atoms loaded on Au surface reach a constant value and will not vary even with further increasing the Pd precursor. Notably, the as-synthesized Au–Pd NCs have the following atom arrangement: Au core/Au–Pd NSA layer/Pd shell with 1 ML. Therefore, a novel core@NSA@$shell_{ML}$ i.e. Au@AuPd@Pd_{ML} nanostructure is facilely and self-controlled synthesized. Compared with other methods, our approach has the following advantages. First, because the catalytic effect depends on the exposed Au atoms on the surface of Au NCs, only one monolayer of Pd shell can be obtained on the outmost surface. Even if NSA layer is firstly formed, the exposed Au atoms in the NSA layer can still catalyze the reduction of Pd precursor, which lead to the continual deposition to form a Pd monolayer on the surface of NSA until all the surface Au atoms are completely covered. Second, this synthesis strategy is simple, rapid, controllable, and without harsh conditions such as high temperature, high pressure, using strong acid/alkali reagents, etc. More importantly, due to self-limiting effect induced by Au catalysis, the loading amount of Pd atoms on the surface of Au core can be conveniently controlled by surface Au content. To our knowledge, we demonstrate for the first time the deposition of Pd on the Au core with a structure evolution from Au@AuPd to Au@AuPd@Pd_{ML} by our synthesis approach, but without the formation of simple Au@Pd_{ML} structure as reported.

In the present work, the synthesized Au–Pd NCs were used for the catalytic conversion of Cr(VI) to Cr(III) by using HCOOH as reductant. We found that the Au@AuPd@Pd_{ML} NCs have the superior catalytic activity in the reduction of Cr(VI) by HCOOH even at room temperature. The obtained turnover frequency (TOF) is even the best one among the reported Pd-based catalysts, to the best of our knowledge. Moreover, the results indicate that the catalytic activity of Au–Pd NCs greatly depends on the Pd atomic geometry of interface surface.

2. Experimental section

2.1. Synthesis of the Au and Pd NCs

The synthesis of the Au and Pd NCs is based on the reported method [27]. For the Au NC synthesis, 50 mL H_2O with 0.0025 g PVP was heated to boiling. 1 mL $HAuCl_4$ (1%) was dropped into the above solution under rigorous stirring for 3 min, and then 1.5 mL sodium citrate (1%) was rapidly added into the solution. After reaction for 1 h, the solution was cooled down to room temperature. Finally, the obtained solution was washed twice by water and purified by centrifugation. In the synthesis of Pd NCs, 0.0025 g PVP was mixed with 20 mL H_2PdCl_4 aqueous solution (2.94 mM). Then 1.5 mL 0.132 M $NaBH_4$ was dropped into the mixture solution under rigorous stirring for 30 min at room temperature. At last, the solution was washed twice with water and purified by centrifugation.

2.2. Self-limiting synthesis of Au@AuPd@PdML core–shell NCs

A seed-mediated preparation method was used to synthesize Au@AuPd@Pd_{ML} NCs. Au NCs with 14 nm in diameter were first mixed with HEPPSO buffer (pH 7.5) to form a 9 mL of mixed solution. Subsequently, 1 mL H_2PdCl_4 solution was introduced. The final concentrations of Au NCs, HEPPSO, and Pd(II) ions are 2 nM, 15 mM and 1 mM, respectively. The reaction mixture was incubated at room temperature for 2 h, and then centrifuged twice to remove superfluous Pd (II) ions. Purified Au@AuPd@Pd_{ML} NCs were finally obtained and stored in water. To investigate the influence of Pd(II) concentration on the synthesis, Au–Pd NCs with different Pd contents were obtained following the same synthesis procedure, and their properties were investigated.

2.3. Verification test

For demonstrating the feasibility of the designed self-limiting growth procedure, the reduction of Pd(II) ions by HEPPSO in the absence of Au NCs or presence of Pd NCs was also examined. We firstly studied whether Pd(II) ions can be reduced by the HEPPSO itself or not. To this end, Pd(II) ions were mixed with HEPPSO (pH 7.5) under stirring, and the final concentrations of Pd(II) ions and HEPPSO are 1 and 15 mM, respectively. As a control experiment, Pd NCs were added into the above mixed solution to examine if Pd(II) ions can be reduced by HEPPSO with the presence of Pd NCs.

2.4. Electrochemical measurements

Electrochemical experiments were carried out for further exploring the surface component distribution of various Au-Pd NCs with different Pd contents. The electrochemical experimental conditions and procedures were chosen and performed according to the literature [26]. In the experiments, the potential range was set from −0.8 to 0.6 V (vs Ag/AgCl). For all the studied samples, after stable cyclic voltammetric (CV)

curves were achieved, the CVs were recorded. All measurements were operated at room temperature.

2.5. Conversion of Cr(VI) under the catalysis of Au–Pd NCs

10 mL mixed solution containing $K_2Cr_2O_7$ (2 mM) and HCOOH (0.45 M) was stirred at room temperature for 10 min. Then a certain amount of catalyst was added into the above solution to study the conversion of Cr(VI) under the catalysis of the Au–Pd NCs. At each designed interval, 50 μL of the solution was taken out and diluted to 1 mL for UV–vis measurement. Under above experimental procedures, commercial Pd black and Pd NCs were used for the Cr(VI) conversion as a comparison. For the recycle experiments, the catalyst was added into a 10 mL of mixed solution containing 2 mM $K_2Cr_2O_7$ and 0.45 M HCOOH. After the above reaction was finished, another Cr(VI) with the same concentration was introduced to repeat the catalytic reaction.

3. Results and discussion

3.1. Self-limiting synthesis of Au–Pd core–shell NCs

To demonstrate the feasibility of our proposed self-limiting protocol, we firstly examined if Pd(II) can be reduced by HEPPSO without the presence of Au NCs. The UV–vis absorption spectra of H_2PdCl_4 solutions at different conditions are shown in Fig. S1. There appears an absorption peak at 425 nm (the black curve) that corresponds to Pd(II) ions [28]. When Pd(II) ions were introduced into the HEPPSO solution, the absorption peak intensity at 425 nm decreases and a new peak at about 382 nm appears (the red curve), which could be ascribed to the complex formed from the coordination of HEPPSO with Pd(II) ions [29]. The absorption spectrum did not change even if the solution was placed for 24 h, and the absorption profile is very different from that of Pd NCs (the green curve) [30]. Further, when Pd NCs were added into the mixed solution of HEPPSO and Pd(II) ions (the blue curve), the absorption spectrum of the mixed solution also presents no change as increasing the reaction time up to 12 h. The above results demonstrate that HEPPSO holds no reducing ability for Pd(II) ions by itself (shown in Fig. 1A), even in the presence of Pd NCs (shown in Fig. 1B).

By contrast, in the presence of Au NCs, the interactions of Pd(II) ions and HEPPSO were studied, and the UV–vis absorption spectra are shown in Fig. 2A. There is only one characteristic absorption peak of Au NCs at 520 nm (the black curve). After enough Pd(II) ions were added, the absorption peak of Au NCs shows a red-shift by 2 nm, resulting from the change of local dielectric constant near the metal core [31]. Meanwhile, the absorption peak of Pd(II) ions also appears in the mixed solution (the red curve). When HEPPSO was introduced, the absorption peak of Au NCs shows a blue shift and decreased intensity (the green curve). After 5 min, the Au NC peak blue-shifts by approximately 4 nm with an obvious decrease of peak intensity (the blue curve), and the absorptive intensity of the Pd(II) ions appears a small decrease, suggesting that a portion of Pd(II) ions is reduced by the Au catalytic system and the Pd atoms are decorated on the surface of Au NCs [32,33]. Subsequently, the spectrum of the mixture keeps unchanged after a 2-h incubation time (the dark yellow curve).

In the following studies, different concentrations of Pd(II) ions were added into the mixed solution of Au NCs and HEPPSO with keeping the overall concentration constant. The UV–vis spectra are shown in Fig. 2B. It can be seen that the absorption peak from Au core gradually blue-shifts with the increase of Pd(II) ion concentration, which can be ascribed to the increase of the electron density in Au NCs induced by the Pd deposition. Meanwhile, the peak intensity gradually decreases, suggesting that more Pd atoms are deposited on the surface of Au cores. However, with further increasing the concentration of Pd(II) ions, the absorption peak of Au–Pd NCs shows no change, which suggests no longer increase of shell thickness. According to the literature [34], the ratio of the peak intensity to that at the half peak width can be used to display the growth of Pd shell on the Au NCs. As shown in Fig. 2B inset, when the added Pd(II) ions reach a certain concentration (such as 600 μM Pd(II) ions vs 2 nM Au NCs), the Pd shell will not continue to grow. These results strongly suggest that the loading amount of Pd in Au@Pd core–shell NCs should be self-controlled due to a self-limiting process.

3.2. Characterizations

A series of characterizations were performed to further demonstrate

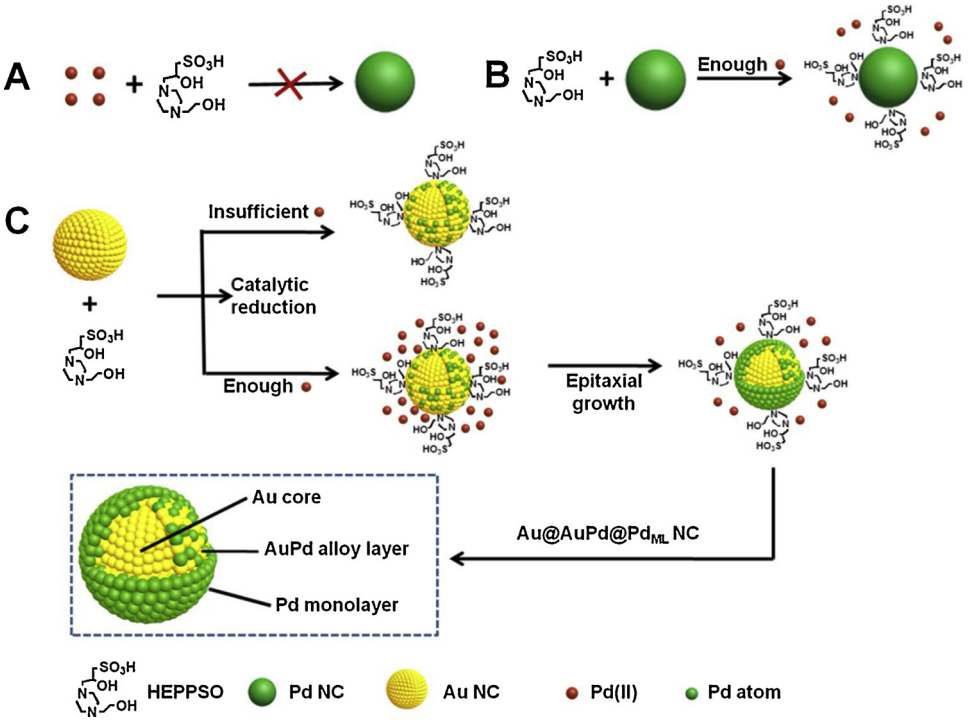

Fig. 1. Schematic representation for the synthesis of Au@AuPd@Pd$_{ML}$ NCs by a self-limiting process. HEPPSO holds no reducing ability for Pd(II) ions (A) and in the presence of Pd NCs (B). (C) With the presence of insufficient Pd(II) ions, Au@AuPd nanostructure is obtained in the mixture of Au NCs and HEPPSO; accordingly, with the presence of enough Pd(II) ions, Au–Pd NCs are obtained with the structure changed from Au@AuPd to Au@AuPd@Pd$_{ML}$.

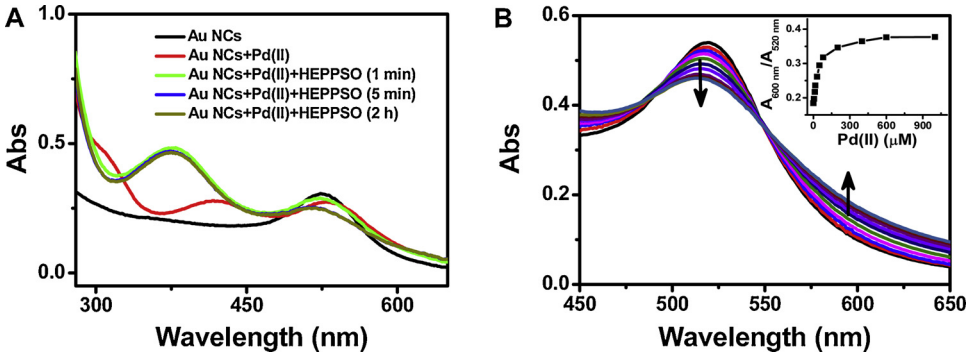

Fig. 2. The UV–vis spectra of (A) the different mixed solutions and (B) the mixtures of Au NCs and HEPPSO with different concentrations of Pd(II) ions. The inset in B represents the relationship between absorption intensity ratio of Au–Pd NCs (at 600 vs at 520 nm) and the concentration of Pd(II) ions in the reaction solution. The concentrations of Au NCs and HEPPSO are 2 nM and 15 mM, respectively. The concentrations of Pd(II) ions are 0, 5, 12, 16, 30, 50, 80, 200, 400, 600 and 1000 μM, respectively. (For interpretation of the references to color in the text, the reader is referred to the web version of this article.).

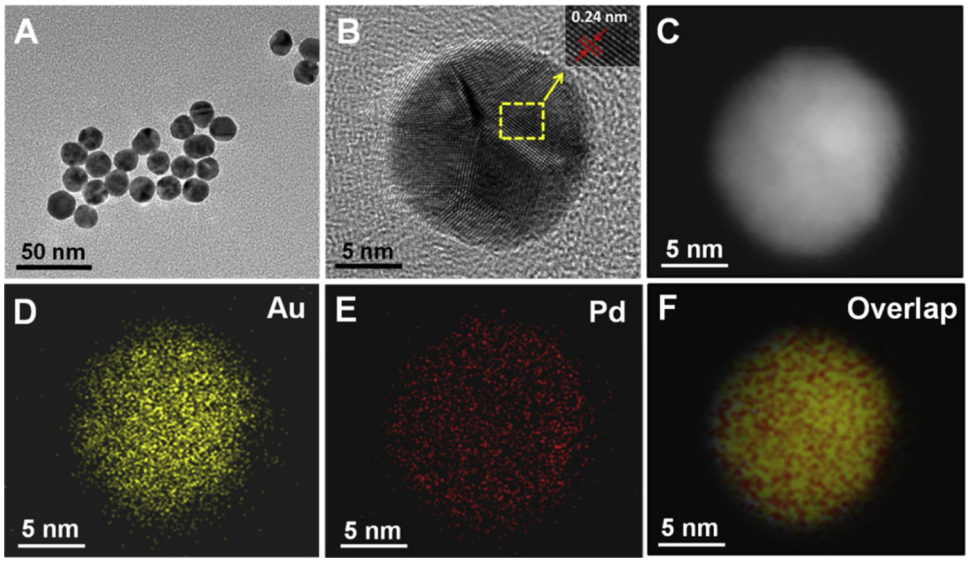

Fig. 3. TEM (A) and HRTEM (B) images of Au–Pd NCs with the most Pd content, STEM image of a single Au–Pd NC (C), and the elemental mapping images of Au (D), Pd (E) and overlap of Au and Pd (F).

the configuration of Au–Pd core–shell NCs, as well as to probe the arrangement of the Pd atoms on the surface of Au core. The inductively coupled plasma-mass spectrum (ICP-MS) was firstly used to determine the Pd content in Au–Pd NCs, as shown in Table S1. With increasing Pd (II) ions in the reaction solution, Pd content increases in Au–Pd NCs. Ultimately, there are the most Pd content of 9.69% (Pd/Au mass ratio) in Au–Pd NCs, again demonstrating that this reaction is self-limiting. In the following characterizations, we mainly investigated the morphology and composition of Au–Pd NCs with the most Pd content. Fig. S2 shows the transmission electron microscopy (TEM) and high resolution TEM (HRTEM) images of the as-synthesized Au seeds, which present spherical and nearly mono-dispersed nanocrystals with an average diameter about 14.04 nm. In the HRTEM image, the main lattice fringes with interplanar spacing of 2.4 Å correspond to the Au (111) crystal plane. After the decoration of enough Pd atoms on the surface of Au NCs to form Au-Pd NCs, the corresponding TEM and HRTEM images are shown in Figs. 3A, B and S3. The average diameter of particles slightly increases to 14.90 nm, and the main lattice fringes of Au–Pd NCs show almost no change compared with the Au seeds. The powder X-ray diffraction (XRD) measurements were also carried out to examine the crystal structures of the two kinds of NCs (Fig. S4). Clearly, no Pd diffraction peaks are observed in the Au–Pd NCs, indicating that no isolated Pd clusters or crystals are formed in the synthesis process and only very thin Pd layer is deposited on the surface of Au seeds [35,36]. To determine the component and distribution of elements in the Au–Pd NCs, the energy-dispersive X-ray spectroscopy (EDX) and high-angle annular dark-field scanning transmission electron microscopy (HAADF-STEM) were further measured. The EDX analysis indicates there presents a fairly small amount of Pd in the Au–Pd NCs (Fig. S5). Meanwhile, from the HAADF-STEM and the corresponding elemental mapping images shown in Fig. 3C–F, the Pd and Au signals can be clearly observed, and Au is mainly located in the core and Pd is only dispersed on the surface of the NCs. Such Au–Pd structure is further demonstrated by the line profile of a single Au–Pd NC (Fig. S6), which states that an ultrathin Pd shell has been coated on the surface of Au seed.

Further, the cyclic voltammetry (CV) measurements are used to characterize the surface composition of the Au–Pd NCs. The CVs of the Au–Pd NCs with different Pd/Au mass ratios are shown in Fig. 4 within the potential range of −0.8 to 0.6 V. It can be seen that without Pd(II) ions added, there is an obvious voltammetric feature of Au for the pure Au NCs (the black curve). With increasing Pd content in the Au–Pd NCs, the peak intensity from Au gradually decreases, and at last disappears. Meanwhile, the voltammetric peaks from Pd gradually increases. According to the CV results, the relative Pd atomic content on the surface can be calculated based on the following equation: $m_R = S_{Pd}/(S_{Pd} + S_{Au})$, where m_R, S_{Pd} and S_{Au} refer to the relative content of Pd, and the integrated reduction peak intensity from Pd and Au oxides in the CVs, respectively [37]. Calculation results are listed in Table S2.

Further, combining the data shown in Fig. 4, Table S1 and S2, we can gain a deeper understanding of the surface and interface structure of Au–Pd NCs. As mentioned above, with the present Au catalytic synthesis strategy, only one Pd monolayer should be ultimately formed on the outer surface of Au–Pd NCs. Here, assuming only the formation of unique Pd shell structure, the shell thicknesses with different Pd contents in Au–Pd NCs were calculated according to the data measured

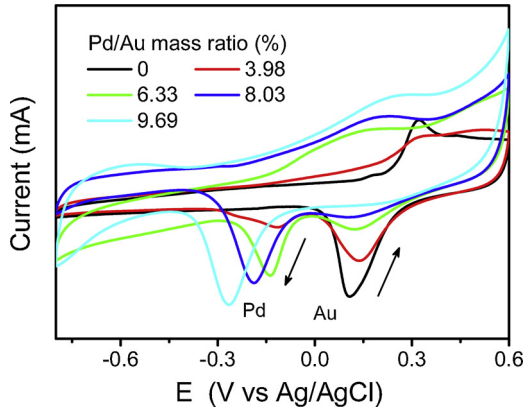

Fig. 4. CV curves of the as-synthesized Au–Pd NCs with different mass ratios of Pd/Au measured in 0.1 M KOH at a scan rate of 100 mV/s. (For interpretation of the references to color in the text, the reader is referred to the web version of this article.).

by ICP-MS, as shown in Table S1 (the calculated details are shown in Supporting information). With increasing Pd content from 0.39 to 9.69% in Au–Pd NCs, the calculated thicknesses of Pd shell change from 0.1 to 2.5 atomic layers on the Au core surface. For instance, when the mass ratio of Pd/Au is 3.98%, the Pd shell with 1 ML should be exactly formed on the Au core (Table S1), which means Au core surface is completely covered by Pd atoms, and no Au atoms are exposed on the surface. However, according to the CV data (the red curve in Fig. 4), there are 69.4% of Au and 31.6% Pd exposed on the outermost surface of particle, respectively (Table S2). The contradictory results suggest that there presents an alloy of Au and Pd on outer surface of Au–Pd NCs, defined as a Au@AuPd but not Au@Pd_{ML} structure. Similarly, with increasing the Pd content to 8.03%, a calculated 2.1 MLs of Pd shell should be covered on the Au surface (Table S1), but in fact, there still has 26.8% of Au exposed (the blue curve in Fig. 4 and Table S2), suggesting that the Pd shell is still less than 1 ML on the outer surface of Au–Pd NCs. Only when the Pd content reaches the maximum in the Au–Pd NCs (9.69% of Pd), the Au–Pd NCs show no CV feature of Au (the cyan curve in the Fig. 4), which indicates that the decorated amount of Pd on the surface is just 1 ML, but not 2.5 MLs from the calculated data in Table S1. The above results clearly indicate that the growth of Pd shell on Au core surface, by this self-limiting procedure, firstly forms AuPd alloy layer interface, and at last produce the Au@AuPd@Pd_{ML} structure (denoted as NSA/ML). The self-limiting synthesis for Au–Pd NCs with NSA/ML structure is illustrated schematically in Fig. 1C, which clearly represent the structure evolution.

Also, we try to illustrate the atomic arrangement in the Au–Pd NCs by this Au–catalytic self-limiting synthesis strategy. In general, the surface of Au NCs contains various kinds of defects such as vacancies, corners and edges, which usually are the active sites with the highest catalytic activity [38,39]. Therefore, in the initial stage, the Pd(II) ions located at these active sites can firstly be reduced and inclined to be decorated at these sites, leading to a much instable Au–Pd composite. Driven by the stable ordered structure, the Au atoms would diffuse from the inside to the surface and meanwhile the Pd atoms would be incorporated into the inside to make the surface reconstruction. When this alloying process i.e. NSA layer reaches a balance, the additional Pd atoms begin to decorate on the particle surface, until a Pd ML is formed. The NSA/ML shell structure is eventually obtained. Consequently, the Au–Pd NCs with NSA/ML shell structure can be easily formed by the present self-limited synthesis procedure based on the Au-catalytic strategy.

In addition, because the difference between alloy and core-shell structures makes the interaction of Au and Pd atoms transform from ligand effect to strain effect, the electronic properties of Au and Pd should change accordingly [40–43]. Thus, the X-ray photoelectron spectroscopy (XPS) of Au–Pd NCs with different loading amount of Pd was further studied. The high-resolution Pd 3d spectrum of the Au@AuPd@Pd_{ML} NCs shown in Fig. 5A displays the presence of zero-valent Pd. Moreover, from the XPS spectra of Au–Pd NCs with different Pd contents, we can see that the peak positions of Pd 3d (Fig. 5B) and Au 4f (Fig. 5C) show obvious shifts with the change of Pd contents. For clearly displaying the evolution of these Au-Pd NCs, the dependence of binding energies of Pd ($3d_{5/2}$) and Au ($4f_{7/2}$) on the Pd content in the Au-Pd NCs are shown in Fig. 5D. It can be seen that the similar trends of the binding energy change can be obtained for both Pd $3d_{5/2}$ and Au

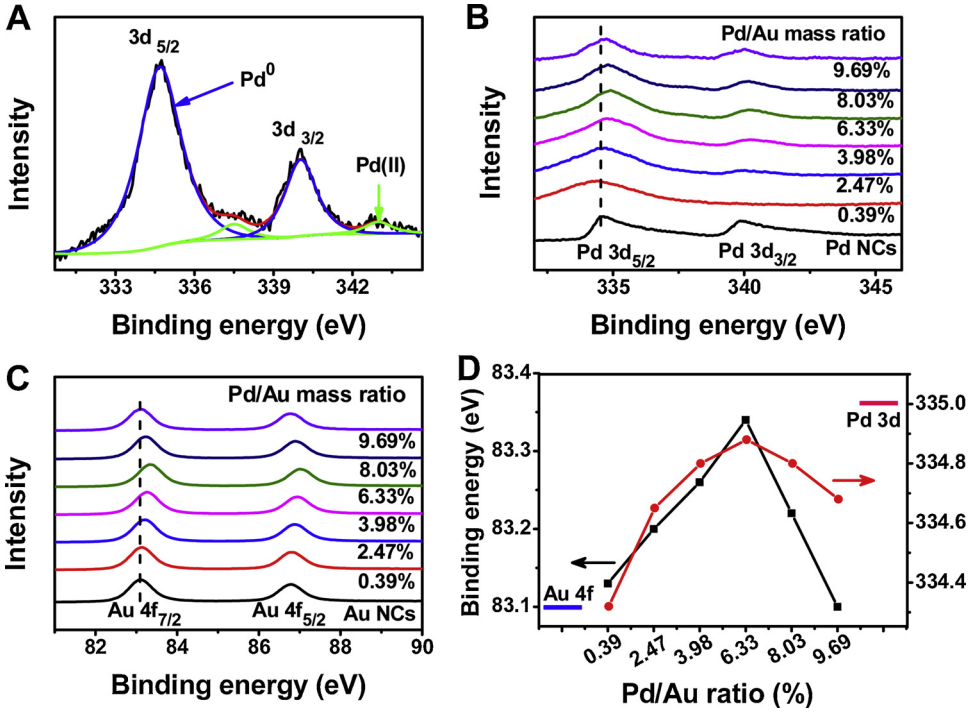

Fig. 5. A. High resolution Pd 3d XPS of Au@AuPd@Pd_{ML} NCs; high resolution Pd 3d (B) and Au 4f (C) XPS spectra of Au–Pd NCs with different Pd contents; the binding energies of Au $4f_{7/2}$ and Pd $3d_{5/2}$ in the Au–Pd NCs as a function of the loading amount of Pd with Pd/Au mass ratios of 0.39, 2.47, 3.98, 6.33, 8.03 and 9.69%, and the blue and magenta bars represent the binding energy of Au $4f_{7/2}$ in the Au NCs and the binding energy of Pd $3d_{5/2}$ in the Pd NCs, respectively. (For interpretation of the references to colour in this figure legend, the reader is referred to the web version of this article).

$4f_{7/2}$, that is the binding energies have positive shift firstly and then negative shift with increasing Pd content. However, for the Au 4f binding energies in Au-Pd NCs, the electron transfer from Au to Pd atoms in the Au–Pd interface induces an overall positive shift (the black dot line in Fig. 5D), compared to that of Au NCs (the blue bar). By contrast, the binding energies of Pd 3d have an overall negative shift (the red dot line) relative to that of Pd NCs (the magenta bar) [44,45]. More notably, the binding energies of Au 4f and Pd 3d don't vary linearly with the increase of Pd content. For the Pd 3d binding energy, when the Pd/Au ratio is low (for example 0.39% shown in Fig. 5D), the Pd $3d_{5/2}$ binding energy shows the most negative shift, relative to that of Pd NCs. With the increase of Pd content, the binding energy of Pd 3d begins to gradually approach to and then shift away from that of Pd NCs. Conversely, the binding energy of the Au 4f gradually shifts away from and then approaches to that of Au NCs. The existence of inflection points in the curves also suggests the change of atomic arrangement in the formed NSA/ML shell.

Next, we try to elucidate the evolution of binding energies of Pd 3d in Au–Pd NCs through the change of the electronic properties in the formation process from NSA to NSA/ML structure. At the formation stage of NSA structure, with the lowest content of Pd in Au–Pd NCs, the amount of Au atoms surrounding the Pd atom is the maximum. On this condition, the influence on Pd atoms imposed by Au atoms is the biggest, leading to the most negative shift of Pd 3d binding energies [46]. With the increase of Pd content (before the inflection point in Fig. 5D), the interaction between Au and Pd atoms gradually weakens due to the dilution of the increased Pd atoms [46], and therefore the shift of binding energies of Pd in Au–Pd NCs becomes smaller and smaller. After the formation of AuPd alloy layer, the ML Pd shell begins to form on the surface of NSA. At this stage, the strain effects induced by the monolayer Pd shell will occur. Consequently, the increase of the density of states at the Fermi level is easier to 'ionize' the metal, resulting in the decrease of the binding energy of Pd [45,47]. Thus, with increasing Pd content (after the inflection point), the binding energies of Pd in Au–Pd NCs are again far away from that of pure Pd NCs, because the strain effect becomes more and more significant. Similarly, the binding energies of Au 4f are first increase, and then decrease, compared to that of Au NCs. The above results indicate that the dominant role of Pd for determining the electronic structure of Au@AuPd@Pd_{ML} NCs undergoes a very meaningful evolution from ligand effect to strain effect.

3.3. Catalytic conversion of Cr(VI)

The dichromate ($Cr_2O_7^{2-}$) ion was selected as the Cr(VI) source because it has a typical absorption peak at 350 nm (coming from ligand to metal charge transfer), whereas the product of Cr(III) shows no absorption. Thus, the reaction can be easily to be monitored by measuring the absorption change of Cr(VI).

In the absence of the Au@AuPd@Pd_{ML} NCs, the absorption intensity of the mixture of $Cr_2O_7^{2-}$ (2 mM) and HCOOH (0.45 M) at 350 nm doesn't change during the 29-h monitoring period, suggesting that the reduction reaction cannot occur without the catalyst (Fig. S7). In contrast, the absorption intensity at 350 nm rapidly decreases and then disappears within 3 min after the addition of the Au@AuPd@Pd_{ML} NCs into the solution (Fig. 6A). The catalytic reaction can be visually verified from the color change of the product solution from yellow to colorless. After adding NaOH, the colorless solution changes to green (Fig. 6A inset), indicating the existence of Cr(III). For comparison, the Pd NCs and commercial Pd black were used as catalysts for the reaction. As shown in Fig. 6B, C, the catalytic reduction times for conversion from Cr(VI) to Cr(III) are 25 and 100 min, respectively, which are 8 and 33 times longer than that with Au@AuPd@Pd_{ML} NCs. The reaction rate (k) was then calculated to further estimate the catalytic activity of Au@AuPd@Pd_{ML} NCs, based on the equation of $-ln(C_t/C_0) = kt$ [6]. From Fig. 6D, the k constants are calculated to be 1.025, 0.119 and 0.024 min^{-1} for Au@AuPd@Pd_{ML} NCs, Pd NCs and Pd black, respectively. The results demonstrate again the much enhanced catalytic activity of Au@AuPd@Pd_{ML} NCs in the conversion of Cr(VI). Recycle experiments were also performed to evaluate the reusability of the Au@AuPd@Pd_{ML} NCs in the practical applications [48,49]. As shown in Fig. S8, after eight cycles, the catalytic activity of the NCs shows no obvious loss, demonstrating the excellent stability of the Au@AuPd@Pd_{ML} NCs. Futhermore, the Au@AuPd@Pd_{ML} NCs for catalytic conversion of Cr(VI) with changing experimental conditions have been studied (the data shown in Fig. S9). For example, under the experimental conditions of 5 mM $Cr_2O_7^{2-}$, 2.3 M HCOOH and 50 °C, the catalytic reaction is completed within 1.5–2.0 min. The results indicate that the reaction time on Cr(VI) conversion are greatly affected by the initial concentration of Cr(VI), the concentration of reducing agent (HCOOH), and catalytic temperature. The above experiments also show that AuPd binary nanostructures can achieve a good catalytic effect on conversion of Cr(VI), which is not only decided by the features of Pd and Au, but also because of the special morphology of nanostructures [5].

Because the surface structure of Au-Pd NCs can be regulated from NSA to NSA/ML by the present self-limiting process, the catalytic activities of the Au-Pd NCs with different interface structures were further studied for the conversion of Cr(VI). By comparison, the conversion time from Pd NCs (25 min, as shown in Fig. 6B) is much less than that from Au NCs (1800 min, as shown in Fig. S10). Moreover, from Figs. S11–14 and 6 A, with the increase of Pd content in the Au–Pd NCs, the reaction time rapidly decreases from 1800 to 3 min. The above results demonstrate that the efficient reduction of Cr(VI) is from the intrinsic catalytic nature of Pd element, but not from the Au element. In order to evaluate the effects of surface and interface composition and structure on the catalytic activity, we further calculated the turnover frequency (TOF) of Pd on the Cr(VI) reduction, in which, $TOF = N_{Cr(VI)}/(m_{Pd} \times t)$, where $N_{Cr(VI)}$, m_{Pd} and t represent the amount of Cr(VI) (mmol), mass of Pd in Au–Pd NCs (mg) and reaction time (min), respectively. The calculated results based on outer-surface Pd content (according to the CVs shown in Fig. 4 and the data in Table S2) are shown in Fig. 7 and Table S3. The TOFs of Au-Pd NCs with different Pd contents are higher than that of pure Pd NCs, which indicates that introducing Au can greatly increase the catalytic activity of Pd. When the shell structure gradually transforms from NSA to NSA/ML, the TOF shows a leaping increase, and the TOF of Au@AuPd@Pd_{ML} NCs is about 23 times higher than that of Pd NCs. Furthermore, the catalytic activity of Au@AuPd@Pd_{ML} NCs was compared with those of other previously reported Pd-based catalysts (Table S4). Obviously, the calculated reaction rate from the present Au@AuPd@Pd_{ML} NCs is much higher than those obtained from the other catalysts even if our reaction occurs at room temperature (see detail in Supporting information). To the best of our knowledge, the catalytic activity of our prepared Au@AuPd@Pd_{ML} NCs is the highest one so far for the Cr(VI) reduction catalyzed by the Pd-based nanostructures.

4. Conclusions

In summary, we have demonstrated the synthesis of Au–Pd core–shell NCs with a near surface AuPd alloy and monolayer Pd shell structure (i.e. Au@AuPd@Pd_{ML} NCs) could be realized by a self-limiting growth procedure, and such nanostructure exhibited high catalytic performance for the reduction of Cr(VI) to Cr(III). Based on the Au catalysis principle and the interaction between the core-shell interface atoms, the Au atoms of core surface can finely control the arrangement of the shell atoms from Au@AuPd to Au@AuPd@Pd_{ML} nanostructure. It is interesting that these NCs showed interface structure-dependent catalytic properties and there appears a notable improvement of catalytic activity from NSA to NSA/ML structure. Furthermore, The Au@AuPd@Pd_{ML} NCs show the best catalytic activity compared with the reported Pd-based catalysts for the Cr(VI) conversion even if at room temperature. These results prove Au@AuPd@Pd_{ML} NCs is an

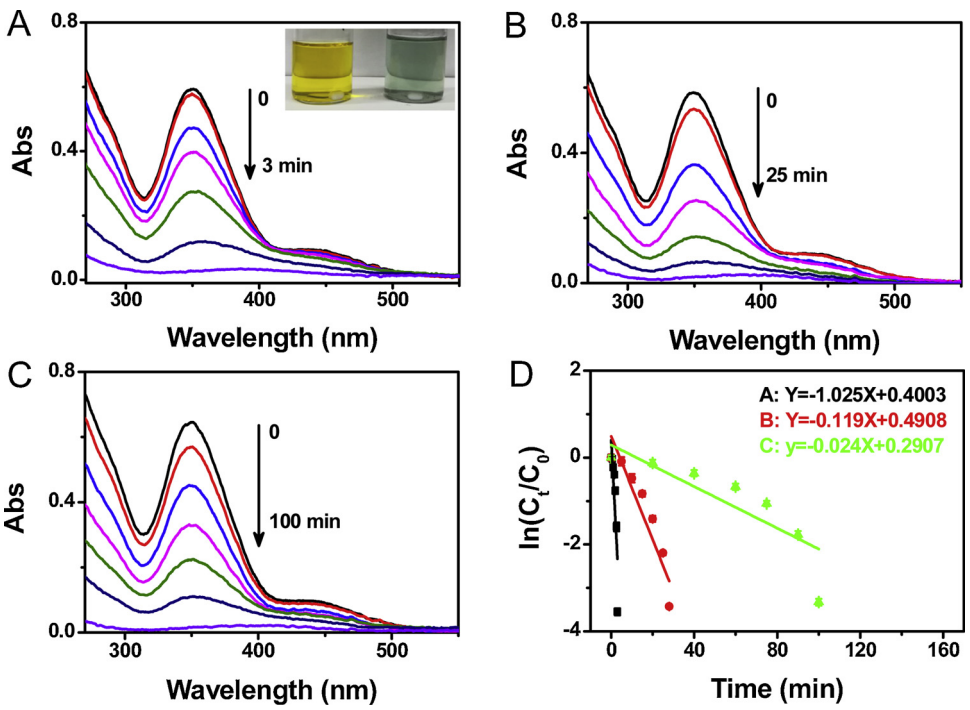

Fig. 6. The absorption spectra obtained in the aqueous solution of 2 mM $K_2Cr_2O_7$ and 0.45 M HCOOH with different catalysts: (A) Au@AuPd@Pd_{ML} NCs, (B) Pd NCs and (C) commercial Pd black. (D) The $ln(C_t/C_0)$ as a function of reaction time with different catalysts. The error bars are standard deviations (n = 5). The inset in (A) shows the photographs of 2 mM $Cr_2O_7^{2-}$ solution (left) and the corresponding product solution after catalytic reaction with the addition of NaOH (right).

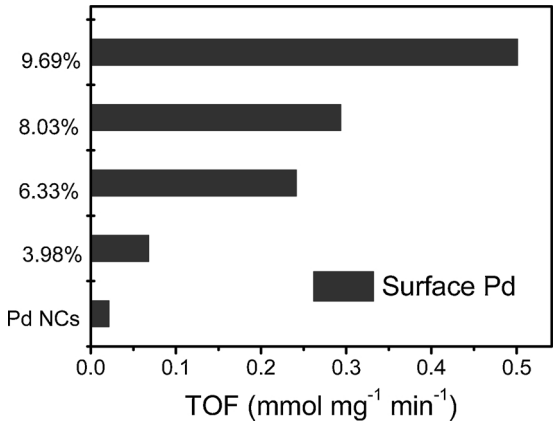

Fig. 7. The TOF as a function of the decorated amount of Pd in the Au–Pd NCs. The Y-axis represents the mass ratio of Pd/Au in the Au–Pd NCs, and Pd NCs.

effective catalyst in remediating Cr(VI)-induced environment problems. Moreover, we hope that this study can inspire further understanding on the structure-activity relationship of core–shell nanostructures to design superior nanocatalysts from the viewpoint of interface construction.

Acknowledgements

This work was supported by the National Natural Science Foundation of China (No. 11874355, 21405149, 21275136, 11374297), National Key Research and Development Plan (No. 2016YFA0203200) and the Natural Science Foundation of Jilin Province, China (No. 20180101222JC).

Appendix A. Supplementary data

Supplementary material related to this article can be found, in the online version, at doi:https://doi.org/10.1016/j.apcatb.2019.04.071.

References

[1] T. Tokunaga, J. Wan, M. Firestone, T. Hazen, E. Schwartz, S. Sutton, M. Newville, Chromium diffusion and reduction in soil aggregates, Environ. Sci. Technol. 35 (2001) 3169–3174.
[2] C. Kim, Q. Zhou, B. Deng, E.C. Thornton, H. Xu, Chromium(VI) reduction by hydrogen sulfide in aqueous media: stoichiometry and kinetics, Environ. Sci. Technol. 35 (2001) 2219–2225.
[3] M. Celebi, M. Yurderi, A. Bulut, M. Kaya, M. Zahmakiran, Palladium nanoparticles supported on amine-functionalized SiO_2 for the catalytic hexavalent chromium reduction, Appl. Catal. B: Environ. 180 (2016) 53–64.
[4] L. Wei, R. Gu, J. Lee, Highly efficient reduction of hexavalent chromium on amino-functionalized palladium nanowires, Appl. Catal. B: Environ. 176 (2015) 325–330.
[5] F. Shao, J. Feng, X. Lin, L. Jiang, A. Wang, Simple fabrication of AuPd@Pd core–shell nanocrystals for effective catalytic reduction of hexavalent chromium, Appl. Catal. B: Environ. 208 (2017) 128–134.
[6] S. Han, J. Bai, H. Liu, J. Zeng, J. Jiang, Y. Chen, J. Lee, One-pot fabrication of hollow and porous Pd–Cu alloy nanospheres and their remarkably improved catalytic performance for hexavalent chromium reduction, ACS Appl. Mater. Interfaces 8 (2016) 30948–30955.
[7] M. Yadav, Q. Xu, Catalytic chromium reduction using formic acid and metal nanoparticles immobilized in a metal–organic framework, Chem. Commun. 49 (2013) 3327–3329.
[8] C. Yang, C. Choi, C. Lee, H. Yi, A facile synthesis-fabrication strategy for integration of catalytically active viral-palladium nanostructures into polymeric hydrogel microparticles via replica molding, ACS Nano 7 (2013) 5032–5044.
[9] K.D. Gilroy, A. Ruditskiy, H.-C. Peng, D. Qin, Y.N. Xia, Bimetallic nanocrystals: syntheses, properties, and applications, Chem. Rev. 116 (2016) 10414–10472.
[10] M. Shao, Q. Chang, J. Dodelet, R. Chenitz, Recent advances in electrocatalysts for oxygen reduction reaction, Chem. Rev. 116 (2016) 3594–3657.
[11] S.T. Hunt, M. Milina, A.C. Alba-Rubio, C.H. Hendon, J.A. Dumesic, Y. Roman-Leshkov, Self-assembly of noble metal monolayers on transition metal carbide nanoparticle, Science 352 (2016) 974–978.
[12] X. Huang, A.J. Shumski, X. Zhang, C.W. Li, Systematic control of redox properties and oxygen reduction reactivity through colloidal ligand-exchange deposition of Pd on Au, J. Am. Chem. Soc. 140 (2018) 8918–8923.
[13] M.B. Gawande, A. Goswami, T. Asefa, H. Guo, A.V. Biradar, D.L. Peng, R. Zboril, R.S. Varma, Core–shell nanoparticles: synthesis and applications in catalysis and electrocatalysis, Chem. Soc. Rev. 44 (2015) 7540–7590.
[14] H. Liao, A. Fisher, Z.J. Xu, Surface segregation in bimetallic nanoparticles: a critical issue in electrocatalyst engineering, Small 11 (2015) 3221–3246.
[15] C.N. Brodsky, A.P. Young, K.C. Ng, C.H. Kuo, C.K. Tsung, Electrochemically induced surface metal migration in well-defined core–shell nanoparticles and its general influence on electrocatalytic reactions, ACS Nano 8 (2014) 9368–9378.
[16] J. Li, H. Yin, X. Li, E. Okunishi, Y. Shen, J. He, Z. Tang, W. Wang, E. Yucelen, C. Li, Y. Gong, L. Gu, S. Miao, L. Liu, J. Luo, Y. Ding, Surface evolution of a Pt–Pd–Au electrocatalyst for stable oxygen reduction, Nat. Energy 2 (2017) 17111.
[17] K. Sasaki, H. Naohara, Y. Choi, Y. Cai, W. Chen, P. Liu, R.R. Adzic, Highly stable Pt monolayer on PdAu nanoparticle electrocatalysts for the oxygen reduction reaction, Nat. Commun. 3 (2012) 1115.

[18] P.P. Fang, Z.T. Tian, C. Amatore, Au–Pd core–shell nanoparticles catalyze Suzuki–Miyaura reactions in water through Pd leaching, Angew. Chem. Int. Ed. 50 (2011) 12184–12188.
[19] Y.N. Xia, K.D. Gilroy, H.-C. Peng, X. Xia, Seed-mediated growth of colloidal metal nanocrystals, Angew. Chem. Int. Ed. 56 (2017) 60–95.
[20] J. Park, L. Zhang, S.-I. Choi, L.T. Roling, N. Lu, J.A. Herron, S. Xie, J. Wang, M.J. Kim, M. Mavrikakis, Y.N. Xia, Atomic layer-by-layer deposition of platinum on palladium octahedra for enhanced catalysts toward the oxygen reduction reaction, ACS Nano 9 (2015) 2635–2647.
[21] C.J. Serpell, J. Cookson, D. Ozkaya, P.D. Beer, Core@shell bimetallic nanoparticle synthesis via anion coordination, Nat. Chem. 3 (2011) 478–483.
[22] W. Luo, C. Zhu, S. Su, D. Li, Y. He, Q. Huang, C. Fan, Self-limiting growth of glucose oxidase-mimicking gold nanoparticles, ACS Nano 4 (2010) 7451–7458.
[23] Y. Wang, W. Liu, X. Yin, Self-limiting growth nanoscale coordination polymers for fluorescence and magnetic resonance dual-modality imaging, Adv. Funct. Mater. 26 (2016) 8463–8470.
[24] D.E. Jesson, G. Chen, K.M. Chen, S.J. Pennycook, Self-limiting growth of strained faceted islands, Phys. Rev. Lett. 80 (1998) 5156–5159.
[25] Y. Ding, F. Fan, Z. Tian, Z.L. Wang, Atomic structure of Au–Pd bimetallic alloyed nanoparticles, J. Am. Chem. Soc. 132 (2010) 12480–12486.
[26] Y. Zhang, X. Li, K. Li, B. Xue, C. Zhang, C. Du, Z. Wu, W. Chen, Novel Au catalysis strategy for the synthesis of Au@Pt core–shell nanoelectrocatalyst with self-controlled quasi-monolayer Pt skin, ACS Appl. Mater. Interfaces 9 (2017) 32688–32697.
[27] X. Wang, G. Meng, C. Zhu, Z. Huang, Y. Qian, K. Sun, X. Zhu, A generic synthetic approach to large-scale pristine-graphene/metal-nanoparticles hybrids, Adv. Funct. Mater. 23 (2013) 5771–5777.
[28] H.-F. Wang, W.E. Kaden, R. Dowler, M. Sterrer, H.-J. Freund, Model oxide-supported metal catalysts-comparison of ultrahigh vacuum and solution based preparation of Pd nanoparticles on a single-crystalline oxide substrate, Phys. Chem. Chem. Phys. 14 (2012) 11525–11533.
[29] L.I. Elding, Palladium(II) halide complexes. I. Stabilities and spectra of palladium (II) chloro and bromo aqua complexes, Inorg. Chim. Acta 6 (1972) 647–651.
[30] B. Lim, M. Jiang, J. Tao, P.H.C. Camargo, Y. Zhu, Y.N. Xia, Shape-controlled synthesis of Pd nanocrystals in aqueous solutions, Adv. Funct. Mater. 19 (2009) 189–200.
[31] Y. Zhang, X. Kong, B. Xue, Q. Zeng, X. Liu, L. Tu, K. Liu, H. Zhang, A versatile synthesis route for metal@SiO_2 core–shell nanoparticles using 11-mercaptoundecanoic acid as primer, J. Mater. Chem. C 1 (2013) 6355–6363.
[32] J. Hu, J. Li, B. Ren, D. Wu, S. Sun, Z. Tian, Palladium-coated gold nanoparticles with a controlled shell thickness used as surface-enhanced Raman scattering substrate, J. Phys. Chem. C 111 (2007) 1105–1112.
[33] Y.W. Lee, M. Kim, Z.H. Kim, S.W. Han, One-step synthesis of Au@Pd core–shell nanooctahedron, J. Am. Chem. Soc. 131 (2009) 17036–17037.
[34] K. Aslan, V.H. Perez-Luna, Surface modification of colloidal gold by chemisorption of alkanethiols in the presence of a nonionic surfactant, Langmuir 18 (2002) 6059–6065.
[35] L.D. Zhu, T.S. Zhao, J.B. Xu, Z.X. Liang, Preparation and characterization of carbon-supported sub-monolayer palladium decorated gold nanoparticles for the electro-oxidation of ethanol in alkaline media, J. Power Sour. 187 (2009) 80–84.
[36] J. Zhang, C. Hou, H. Huang, L. Zhang, Z. Jiang, G. Chen, Y. Jia, Q. Kuang, Z. Xie, L. Zheng, Surfactant-concentration-dependent shape evolution of Au–Pd alloy nanocrystals from rhombic dodecahedron to trisoctahedron and hexoctahedron, Small 9 (2013) 538–544.
[37] A. Habrioux, W. Vogel, M. Guinel, L. Guetaz, K. Servat, B. Kokoh, N. Alonso-Vane, Structural and electrochemical studies of Au–Pt nanoalloys, Phys. Chem. Chem. Phys. 11 (2009) 3573–3579.
[38] H. Zhang, T. Watanabe, M. Okumura, M. Haruta, N. Toshima, Catalytically highly active top gold atom on palladium nanocluster, Nat. Mater. 11 (2012) 49–52.
[39] J. Zhong, X. Jin, L. Meng, X. Wang, H. Su, Z. Yang, C.T. Williams, B. Ren, Probing the electronic and catalytic properties of a bimetallic surface with 3 nm resolution, Nat. Nanotechnol. 12 (2017) 132–137.
[40] L. Bu, N. Zhang, S. Guo, X. Zhang, J. Li, J. Yao, T. Wu, G. Lu, J. Ma, D. Su, X. Huang, Biaxially strained PtPb/Pt core/shell nanoplate boosts oxygen reduction catalysis, Science 354 (2016) 1410–1414.
[41] J.R. Kitchin, J.K. Norskov, M.A. Barteau, J.G. Chen, Role of strain and ligand effects in the modification of the electronic and chemical properties of bimetallic surfaces, Phys. Rev. Lett. 93 (2004) 156801.
[42] C. Wang, X. Sang, J.T.L. Gamler, D.P. Chen, R.R. Unocic, S.E. Skrabalak, Facet-dependent deposition of highly strained alloyed shells on intermetallic nanoparticles for enhanced electrocatalysis, Nano Lett. 17 (2017) 5526–5532.
[43] W. Gao, Z.D. Hood, M. Chi, Interfaces in heterogeneous catalysts: advancing mechanistic understanding through atomic-scale measurements, Acc. Chem. Res. 50 (2017) 787–795.
[44] M.O. Nutt, K.N. Heck, P. Alvarez, M.S. Wong, Improved Pd on Au bimetallic nanoparticle catalysts for aqueous-phase trichloroethene hydrodechlorination, Appl. Catal. B: Environ. 69 (2006) 115–125.
[45] H. Wang, C. Wang, H. Yan, H. Yi, J. Lu, Precisely-controlled synthesis of Au@Pd core–shell bimetallic catalyst via atomic layer deposition for selective oxidation of benzyl alcohol, J. Catal. 324 (2015) 59–68.
[46] C.W. Yi, K. Luo, T. Wei, D.W. Goodman, The composition and structure of Pd–Au surfaces, J. Phys. Chem. B 109 (2005) 18535–18540.
[47] B.T. Sneed, A.P. Young, C.K. Tsung, Building up strain in colloidal metal nanoparticle catalysts, Nanoscale 7 (2015) 12248–12265.
[48] M. Liang, R. Su, W. Qi, Y. Zhang, R. Huang, Y. Yu, L. Wang, Z. He, Reduction of hexavalent chromium using recyclable Pt/Pd nanoparticles immobilized on procyanidin-grafted eggshell membrane, Ind. Eng. Chem. Res. 53 (2014) 13635–13643.
[49] G. Fu, X. Jiang, R. Wu, S. Wei, D. Sun, Y. Tang, T. Lu, Y. Chen, Arginine-assisted synthesis and catalytic properties of single-crystalline palladium tetrapods, ACS Appl. Mater. Interfaces 6 (2014) 22790–22795.